Possibility of Estimation of Multilayer Relaxation at a NiAl(111) Surface Using Computer Simulations of 180° NICISS

Wataru TAKEUCHI

Department of Applied Physics, Faculty of Science, Okayama University of Science, Ridai-cho 1-1, Okayama 700, Japan

(Received September 30, 1995)

The possibility of estimation of the multilayer relaxation with Ni atoms at the topmost layer of a NiAl(111) surface has been examined by using the computer simulations of the 180° neutral impact-collision ion scattering spectroscopy (NICISS). The computer simulations employing the ACOCT program code based on the binary collision approximation (BCA) are performed for the case of 2 keV Li^+ ions incident along the $[\bar{1}2\bar{1}]$ direction of NiAl(111) surface. In the ACOCT results of 180° Li NICISS intensity versus angle of incidence between an ion beam and the target surface, it is found that the peak positions of peaks from not only Ni atoms but also Al atoms are strongly dependent on the relaxation values of first and second interlayer spacings. From these ACOCT results, it is possible to estimate the multilayer relaxation on Ni terminated layer at the NiAl(111) surface with the 180° Li NICISS data.

1. Introduction

Investigations of the surface structure of crystals, e.g. surface relaxation or surface reconstruction etc., have been carried out using low energy ion scattering (LEIS)[1]. The principle of surface structural analysis in LEIS is based on the shadowing effect and the blocking effect of elastic scattering at the surface. In the case of coexistence of both effects, i.e. in the case of the multiple scattering, it is difficult to analyze quantitatively the surface structure, because it is not easy to determine whether the decrease of the backscattered intensity versus an angle of incidence, α, between an ion beam and the target surface is due to the shadowing effect or the blocking effect.

If the analyzer is set to detect the intensity of 180° backscattered ions which make head-on collisions with the target atoms, it is considered that only the shadowing effect occures without the blocking effect, because in $\theta_L = 180°$ the incoming and outgoing trajectories are almost identical, where θ_L denotes the scattering angle. In order to analyze quantitatively the structure of the first few layers at the crystal surface, a specialization of LEIS chosen as $\theta_L = 180°$, i.e. impact-collision ion scattering spectroscopy (ICISS)[2,3], and its variants, i.e. coaxial, alkali-ion and neutral impact-collision ion

scattering spectroscopy (CAICISS[4,5], ALICISS[6-8] and NICISS[7-11], respectively), have been proposed. When an angle of incidence α is attained in which the edge of the shadow cone of an atom passes through the center of a neighbor atom, a sharp enhancement in the 180° backscattering intensity is observed due to both the focusing of the incoming trajectories at the edge of the shadow cone and the focusing of the outgoing trajectories at the edge of the blocking cone.

NiAl is an ordered binary alloy and is extensively used for high temperature and high ductility applications. However, the structure of NiAl(111) surface is still subject of controversy. Since NiAl has the CsCl structure, its bulk (111) layers consist of alternating layers of odered lattices with either all Ni atoms or all Al atoms which are separated by an interlayer spacing of only 0.83 Å and its (111) surface is terminated by either a Ni layer or an Al layer.

After annealing the NiAl at 1400 K, Niehus et al.[12] have investigated the clean NiAl(111) surface with 180° He NICISS data using the time-of-flight (TOF) technique. Consequently, they have pointed out that the clean NiAl(111) surface consists of alternating layers of Ni atoms and Al atoms with Ni atoms at the outermost layer. Since it has been reported that the first interlayer spacing on Ni terminated domain at the NiAl(111) surface is contracted 50% in LEED analysis[13,14] and 38±15% in LEIS analysis[15], Takeuchi and Yamamura[16] have evaluated the relaxation of clean NiAl(111) surface with the 180° He NICISS data measured by Niehus et al.[12] using the ACOCT computer code[17,18] based on the binary collision approximation (BCA). As a result, Takeuchi and Yamamura have obtained that the first interlayer spacing with Ni atoms at the outermost layer of NiAl(111) surface is contracted 40%. The inward relaxation of 40% determined by the ACOCT results is in agreement with the relaxation value obtained in LEED and LEIS analyses.

Recently, the multilayer relaxation of ordered alloy surfaces has been studied by many scientists[19]. Noonan and Davis[13,14] have evaluated the multilayer relaxation on Ni terminated domain at the NiAl(111) surface by an analysis in LEED, and they have obtained that the first and second interlayer spacings are contracted 50% and expanded 15%, respectively. From the 180° He NICISS data measured by the group of Niehus[12], it is not easy to estimate the multilayer relaxation at the NiAl(111) surface, because the 180° He NICISS intensity from Al atoms is considerably smaller than that from Ni atoms and is not strongly dependent on α. If the 180° NICISS data is obtained under the conditions that the increase of the 180° NICISS intensity from Al atoms is advanced and that consequently the dependence of the 180° NICISS intensity from Al atoms on α becomes more remarkably, the possibility exists that we can estimate the multilayer relaxation with Ni atoms at the outermost layer of NiAl(111) surface.

It is desirable to analyze the multilayer relaxation at the NiAl(111) surface by using other methods of measurements besides LEED so as to demonstrate more perfectly the multilayer relaxation at this surface. Thus, the purpose of this paper is to examine whether the estimation of multilayer relaxation on Ni terminated domain at the NiAl(111) surface is possible by analyzing the 180° NICISS intensity data using the

ACOCT simulation code or not. For the sake of the increase of 180° NICISS intensity from Al atoms, we choose Li^+ ions as the projectiles in the present ACOCT code, because the scattering cross section for $Li^+ \rightarrow Al$ is larger than that for $He^+ \rightarrow Al$. The computer simulations of 180° NICISS employing the ACOCT code are performed for the case of 2 keV Li^+ ions incident along the $[\bar{1}2\bar{1}]$ direction of NiAl(111) surface.

2. The ACOCT program

The ACOCT program code was developed to simulate three-dimensionally the atomic collisions in a crystalline target within BCA. The details of ACOCT code are described elsewhere[17,18]. Here, we explain only the main features of the ACOCT code. In the ACOCT code, we used the crystal translational property that the crystal structure is formed when a basis of atoms is attached identically to each lattice point.

The interatomic potential employed in the present calculations is the Molière approximation[20] to the Thomas-Fermi function with the Firsov screening length[21]. Thermal vibrations are taken into account three-dimensionally by using the well-known Einstein model where atoms in the target are considered to move free from each other. A Gaussian distribution is employed for the probability distribution function of thermal displacement. The one-dimensional RMS thermal-vibration amplitude is calculated using the Debye model of the solid[22]. During the 180° He NICISS measurements by Niehus et al.[12], the sample has kept at the temperature $T=150$ K so as to minimize the surface thermal vibrations which reduce the sharpness of the peak slopes in the 180° NICISS intensity against α. Thus, in the present ACOCT code, we deal only with the isotropic vibrations of atoms at the NiAl(111) surface for $T=150$ K.

Here, we must note the differences between the collision time and thermal-vibration periods of the target atoms. In the case of 2 keV Li^+ ions incident on the $[\bar{1}2\bar{1}]$ direction of a NiAl(111) surface, it takes a time of the order of 10^{-15} s to pass between two atoms which make the contributions to the focusing effect for the 180° backscattered trajectory, while the thermal vibration periods of atoms in solids are of the order of 10^{-13} s. Accordingly, it is very resonable to suppose that an atom does not change its position during incoming and outgoing processes of a projectile[16,23-26]. This effect is applied for the present ACOCT code.

In addition, the present ACOCT code is regarded as the simulation program code of a projectile incident only on the $[\bar{1}2\bar{1}]$ axis of a NiAl(111) surface so as to minimize the statistical errors about the intensity of 180° backscattering, because the intensity of 180° backscattered Li particles which make head-on collisions with the target atoms is considerably smaller than that of forward scattering or that of backscattering at $\theta_L < 180°$. Since 180° ICISS employed 2 keV Li^+ alkali-ions as projectiles does not suffer from high neutralization during the scattering processes and at the present day one can perform the 180° NICISS measurements[7-12], the neutralization effect is not incorporated in the present ACOCT program code.

3. ACOCT results and discussion

Previously, it has been pointed out that there are contributions not only of first- or second-layer atoms at the target surface but also of several atomic-layers below the surface to the 180° (N)ICISS intensity[5,26,27]. The NiAl(111) surface has a very open structure. Therefore, the influences from first- to thirteenth-layer atoms on the 180° backscattering are taken into account in the present ACOCT program code. The computer simulations are performed for an acceptance half-angle of the detector, Δ, of 3.0°. Moreover, in the present ACOCT code we regard first-layer atoms at the NiAl(111) surface as all Ni atoms, because in this paper we examine the possibility of estimation of the multilayer relaxation on Ni terminated layer at the NiAl(111) surface with the 180° NICISS data.

The angle of incidence at which the maximum intensity is observed, α_m, is very sensitive to the interatomic potential under the large-angle backscattering condition. Overbury's group[15,28] have used $C_A=0.70$ for Li^+ on Ni and $C_A=0.71$ for Li^+ on Al in LEIS analysis for $Li^+ \rightarrow$NiAl, where C_A is a scaling factor compared to the Firsov screening length in the Molière approximation to the Thomas-Fermi potential. Thus, in the present ACOCT code we employed $C_A=0.70$ for Li^+ on Ni and for Li^+ on Al in the case of 2 keV $Li^+ \rightarrow$NiAl(111).

Fig. 1 shows the ACOCT results of 180° Li NICISS intensity from Ni atoms at the NiAl(111) surface versus the angle of incidence, α, for no relaxation, where $\Delta d_{12}/d_B$ is the relaxation value (in %) of first interlayer spacing, d_{12}, between first- and second-layer atoms defined as $\Delta d_{12}/d_B=(d_{12}-d_B)/d_B$, $\Delta d_{23}/d_B$ is the relaxation value (in %) of second interlayer spacing, d_{23}, between second- and third-layer atoms defined as $\Delta d_{23}/d_B=(d_{23}-d_B)/d_B$, d_B is the bulk interlayer spacing, α is measured from the [1$\bar{2}$1] direction of NiAl(111) surface, and $\alpha=0°$ - 52°. Whereas the first peak is a single peak Ni_1 with the peak position $\alpha_m=11°$, the second peak is splitted into the double peaks

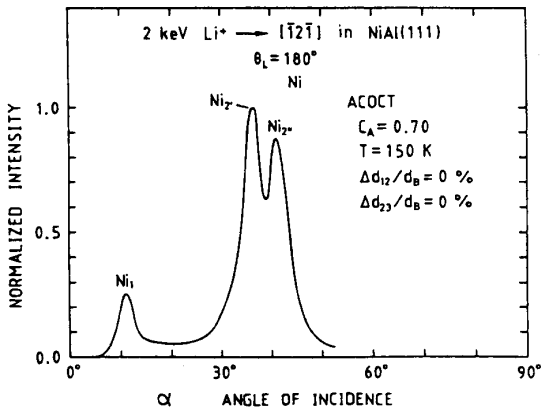

Fig. 1 ACOCT results of 180° Li NICISS intensity from Ni atoms at a NiAl(111) surface versus angle of incidence α for no relaxation.

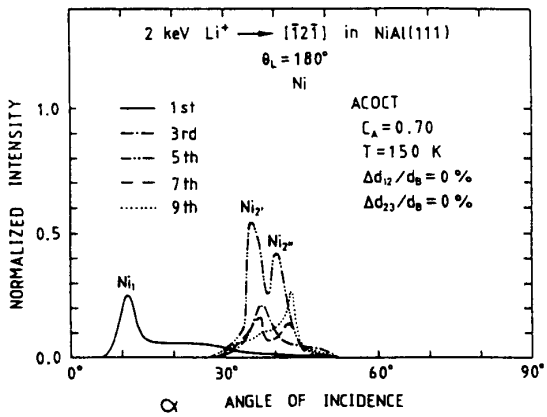

Fig. 2 Simulated 180° Li NICISS intensity from individual Ni atomic-layers at a NiAl(111) surface versus α using the ACOCT code, where the notations Ni_1, Ni_2' and Ni_2'' of peaks are equivalent to those in Fig. 1.

$Ni_{2'}$ with $\alpha_m = 36°$ and $Ni_{2''}$ with $\alpha_m = 41°$. The influences of individual Ni atomic-layers on the 180° Li NICISS intensity in Fig. 1 are depicted in Fig. 2. The intensity peak Ni_1 is due to the 180° backscattering from first-layer Ni atoms. The double peaks of $Ni_{2'}$ and $Ni_{2''}$ result mainly from the contributions of fifth- and seventh-layer Ni atoms.

For the sake of more detailed discussion of the ACOCT results in Fig. 2, the schematic trajectories of 180° Li particles backscattered from the individual Ni atomic-layers are shown in Figs. 3a-3c, where the open and solid circles represent the Ni and Al atoms, respectively. Strictly speaking, the peak intensity of 180° backscattering is due to both the focusing of the incoming trajectories at the edge of the shadow cone and the focusing of the outgoing trajectories at the edge of the blocking cone. Since the incoming and outgoing trajectories for $\theta_L = 180°$ are almost identical, for convenience' sake we adopt the representation of only the focusing of incoming trajectories in the following discussion. From Fig. 3a, it is understood that the peak Ni_1 is attributed to the focusing effect of the incoming trajectories from first-layer Ni atoms onto their first-layer neighbor Ni atoms. As is shown in Fig. 3b, the double peaks of $Ni_{2'}$ and $Ni_{2''}$ result from the two patterns of characteristic 180° trajectories backscattered from fifth-layer Ni atoms, i.e., the peaks $Ni_{2'}$ and $Ni_{2''}$ are due to the focusing effects from fourth-layer Al atoms and from first-layer Ni atoms onto

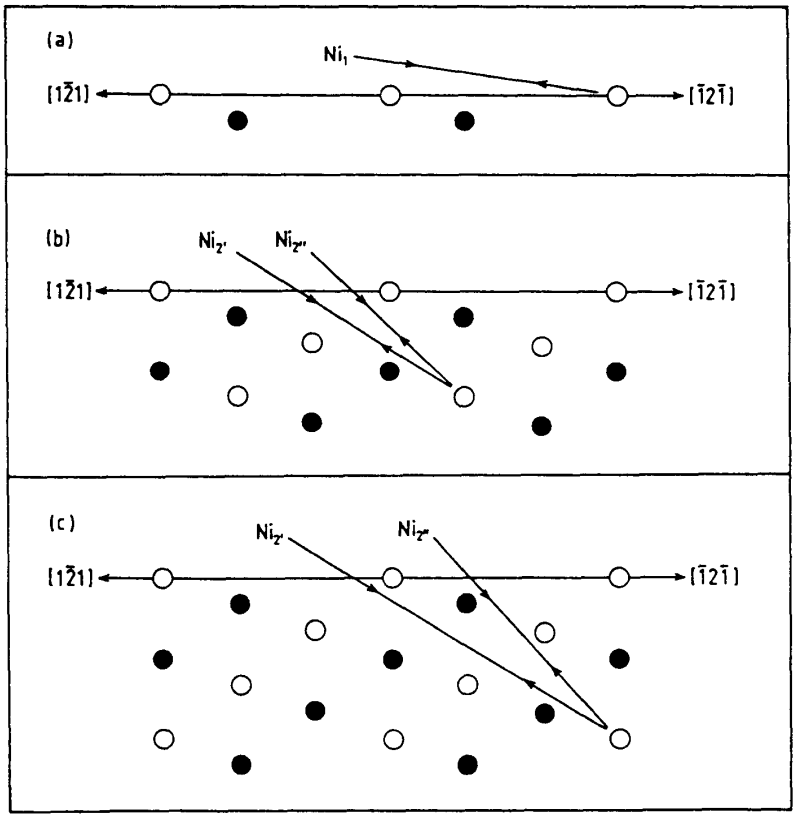

Fig. 3 Schematic trajectories of 180° Li particles backscattered from (a) first-, (b) fifth- and (c) seventh-layer Ni atoms at a NiAl(111) surface, where all notations of trajectories correspond to those of peaks in Fig. 2, and the open and solid circles denote the Ni and Al atoms, respectively.

fifth-layer Ni atoms, respectively. If the surface relaxation is taken into account in the present case, the trajectory Ni_{2}'', i.e. the peak position α_m of peak Ni_{2}'', is especially influenced by the relaxation of first-layer Ni atoms. In Fig. 3c, the double peaks of Ni_{2}' and Ni_{2}'' are due to the focusing effects from first-layer Ni atoms and/or sixth-layer Al atoms and from second-layer Al atoms and/or third-layer Ni atoms onto seventh-layer Ni atoms, respectively. The 180° backscattered trajectory Ni_{2}' from seventh-layer Ni atoms as well as fifth-layer Ni atoms will be also influenced by the relaxation of Ni atoms at the topmost layer. Accordingly, it is supposed that the relaxation of first interlayer spacing drastically affects the profiles of the double peaks of Ni_{2}' and Ni_{2}'' due to the 180° backscattering from fifth- and seventh-layer Ni atoms. The above-mentioned ACOCT results of 180° NICISS intensity from Ni atom for $Li^{+}\rightarrow$ NiAl(111) are very similar to those for $He^{+}\rightarrow$NiAl(111)[16]. In 180° (N)ICISS, the energy loss of a projectile is almost due to the elastic energy loss for the backscattering event when a projectile makes a head-on collision with a target atom. Therefore, in Figs. 3a -3c it is considered that the backscattered energies of 180° Li particles for the trajectory Ni_1 from first-layer Ni atoms, for the trajectories Ni_{2}' and Ni_{2}'' from fifth-layer Ni atoms and for the trajectories Ni_{2}' and Ni_{2}'' from seventh-layer Ni atoms are roughly identical.

Fig. 4 shows the ACOCT results of 180° Li NICISS intensity from Al atoms at the NiAl(111) surface as a function of α for $\alpha = 0° - 52°$, where the surface relaxation is not taken into account in Fig. 4. The 180° Li NICISS intensity from Al atoms is not considerably smaller than that from Ni atoms (see Fig. 1) and is strongly dependent on α. The influences of individual Al atomic-layers on the 180° Li NICISS intensity in Fig. 4 are shown in Fig. 5. The intensity peak Al_1 is mostly due to the focusing effects at second-, fourth- and sixth-layer Al atoms. The trajectories of 180° Li particles backscattered from the individual Al atomic-layers are schematically delineated in Figs. 6a and 6b. As is shown in Fig. 6a, the peak Al_1 is due to the focusing effect from first-layer

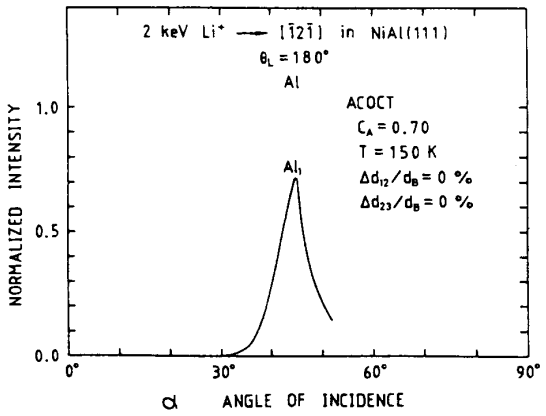

Fig. 4 ACOCT results of 180° Li NICISS intensity from Al atoms at a NiAl(111) surface as a function of α for no relaxation.

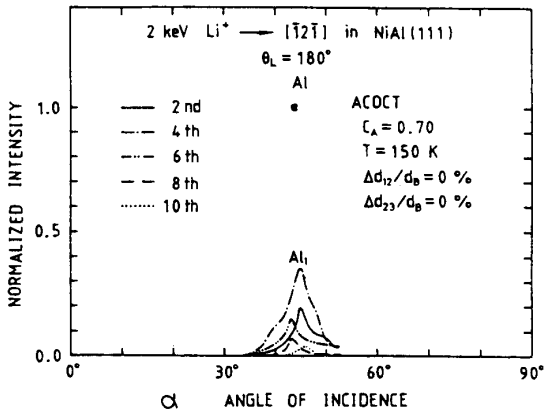

Fig. 5 Simulated 180° Li NICISS intensity from individual Al atomic-layers at a NiAl(111) surface versus α using the ACOCT code, where the notation Al_1 is equivalent to that in Fig. 4.

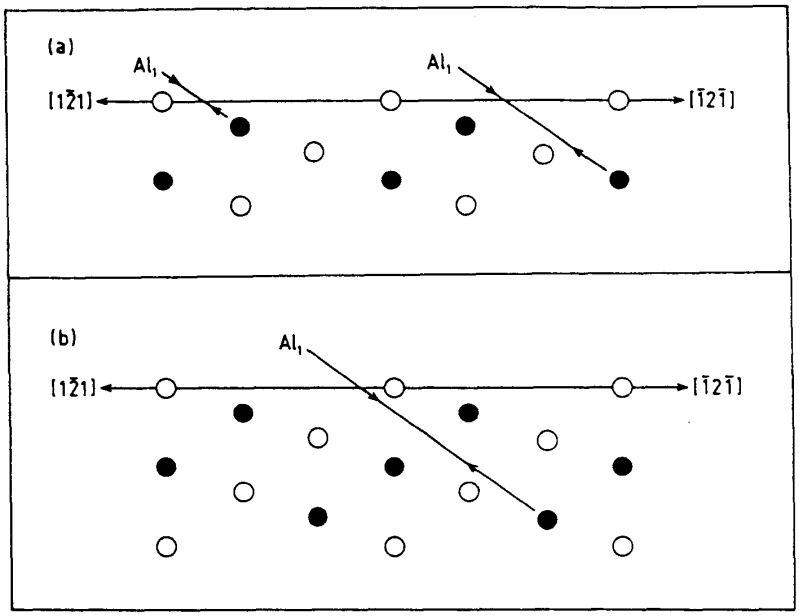

Fig. 6 Schematic trajectories of 180° Li particles backscattered from (a) second- and fourth- and (b) sixth-layer Al atoms at a NiAl(111) surface, where the notation Al_1 of trajectories corresponds to that of peaks in Fig. 5.

Ni atoms onto second-layer Al atoms and results from the focusing effect by third-layer Ni atoms onto fourth-layer Al atoms. From Fig. 6b, it is known that the peak Al_1 is attributed to the focusing effect from first-layer Ni atoms and/or fifth-layer Ni atoms onto sixth-layer Al atoms. Thus, it is imagined that the relaxation of first interlayer spacing affects the trajectory Al_1 from second- and sixth-layer Al atoms.

In the case of the surface structural analysis with 180° (N)ICISS intensity versus α, properly speaking we must determine the shadowing critical angle α_c at which the edge of the shadow cone of an atom passes through the center of a neighbor atom[2,3]. Although the peak position α_m in the 180° (N)ICISS intensity is slightly different from the shadowing critical angle α_c, in practice the structure of NiAl(111) surface is analyzed by using α_m instead of α_c for the sake of two reasons as follows:

(1) It is difficult to determine α_c accurately because of ambiguities due to surface thermal vibrations[23] and due to the value employed as the ratio of the intensity at $\alpha = \alpha_c$ to the peak intensity at $\alpha = \alpha_m$[3,29,30].

(2) The peak position α_m of 180° He NICISS intensity from Ni atoms at the NiAl(111) surface as a function of α is remarkably influenced by the surface relaxation[16].

In the following discussion on the relaxation with Ni atoms at the topmost layer of NiAl(111) surface, we note that for $\alpha = 30° - 50°$ there is the remarkable contribution of surface relaxation to α_m in the 180° Li NICISS intensity from Ni and Al atoms, because the ACOCT results of 180° backscattered intensity from Ni and Al atoms are strongly dependent on α for $\alpha = 30° - 50°$ (see Figs. 1 and 4). Since it has pointed out that the first interlayer spacing on Ni terminated layer at the NiAl(111) surface is contracted 35 - 50%[13-16], Fig. 7 shows the ACOCT results of 180° Li NICISS intensity from Ni atoms versus α for the various inward-relaxation values $\Delta d_{12}/d_B$, where $\Delta d_{23}/$

$d_B=0\%$, and $\alpha=30^\circ$ - 50°. The most noticeable fact in Fig. 7 is that the double peaks of $Ni_{2'}$ and $Ni_{2''}$ for contraction of $\Delta d_{12}/d_B=0$ - 30% change drastically to the single peak Ni_2 for $\Delta d_{12}/d_B=-40\%$.

Here, let us discuss the reasons why the double peaks of $Ni_{2'}$ and $Ni_{2''}$ change to the single peak Ni_2 by using $\Delta d_{12}/d_B=-40\%$ in the ACOCT code. The occurrence of a single peak Ni_2 is mainly due to the focusing effects at fifth- and seventh-layer Ni atoms. The reason of occurrence of single peak Ni_2 attributable to fifth- and seventh-layer Ni atoms is explained as follows. The peak position α_m for the trajectory $Ni_{2''}$ due to the focusing from first-layer Ni atoms onto fifth-layer Ni atoms decreases with increasing the inward relaxation of first interlayer spacing (see Fig. 3b). However, α_m

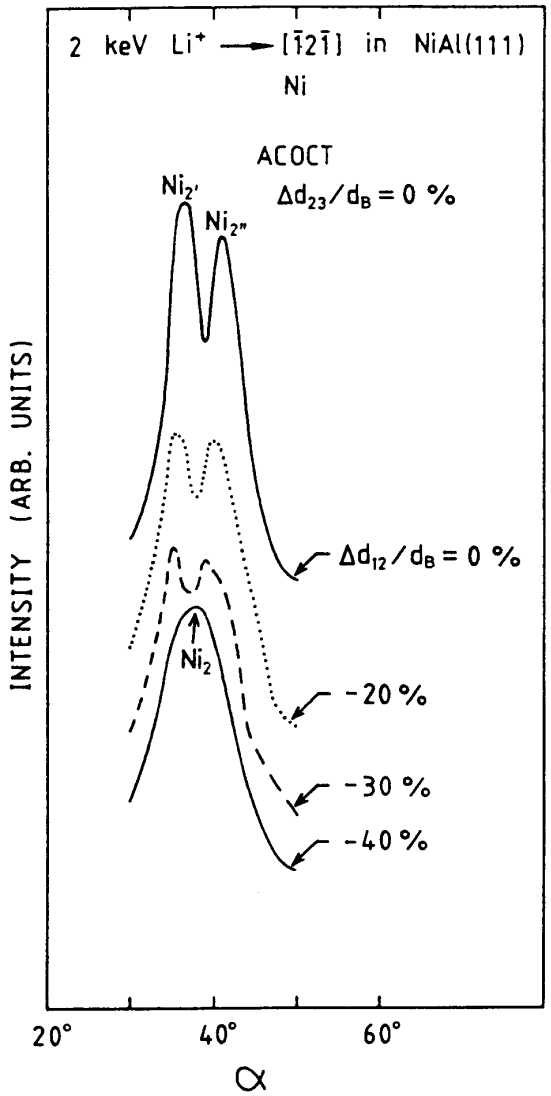

Fig. 7 ACOCT results of dependence of 180° Li NICISS intensity from Ni atoms at a NiAl(111) surface on α for various inward-relaxation values $\Delta d_{12}/d_B$, where the notations $Ni_{2'}$ and $Ni_{2''}$ of peaks correspond to those in Fig. 1.

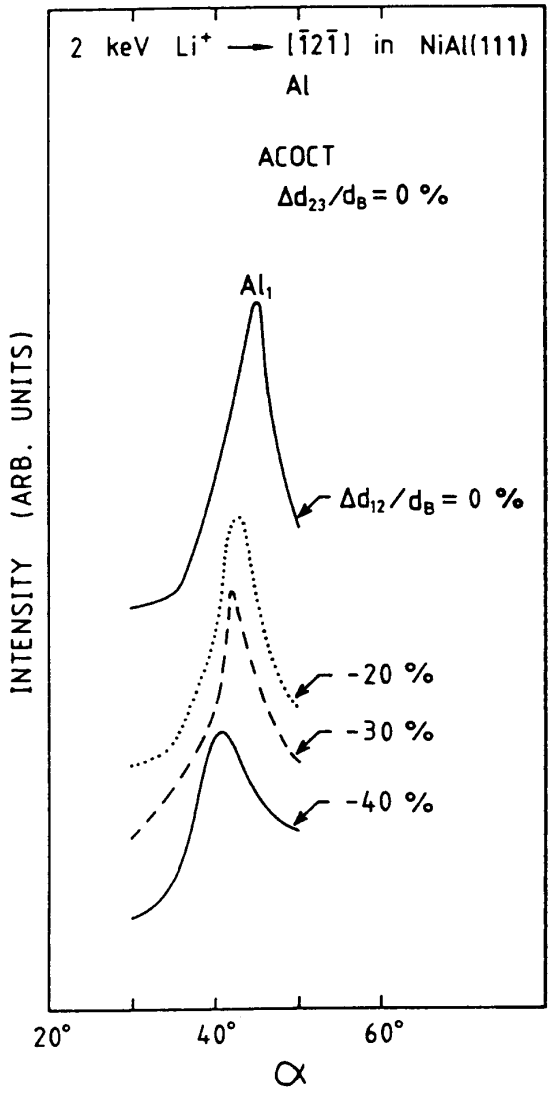

Fig. 8 Simulated 180° Li NICISS intensity from Al atoms at a NiAl(111) surface as a function of α for various inward-relaxation values $\Delta d_{12}/d_B$ using the ACOCT code, where the notation Al_1 of peak corresponds to that in Fig. 4.

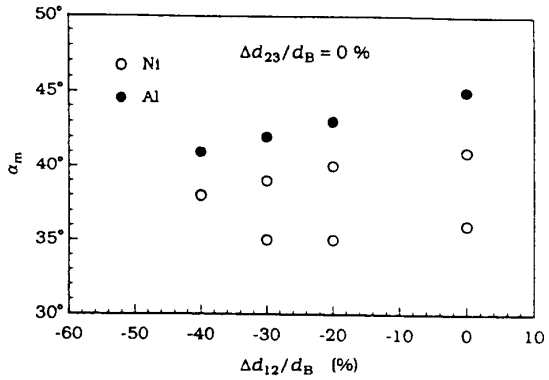

Fig. 9 ACOCT results of peak positions α_m of 180° Li NICISS intensity from Ni and Al atoms at a NiAl(111) surface versus $\Delta d_{12}/d_B$.

for the trajectory $Ni_{2'}$ due to the focusing by fourth-layer Al atoms onto fifth-layer Ni atoms is not affected by the contraction of first interlayer spacing. As a result, in a combination with the trajectories $Ni_{2'}$ and $Ni_{2''}$ of 180° Li particles backscattered from fifth-layer Ni atoms for $\Delta d_{12}/d_B = -40\%$, the superposition of peaks $Ni_{2'}$ and $Ni_{2''}$ produces the single peak Ni_2. The focusing effect from first-layer Ni atoms onto seventh-layer Ni atoms occurs hardly owing to the inward relaxation of first-layer Ni atoms (see Fig. 3c). Thus, in the 180° Li NICISS intensity from seventh-layer Ni atoms for the contraction of first interlayer spacing, the peak $Ni_{2'}$ disappears and only the peak $Ni_{2''}$, i.e. only the peak Ni_2, exsits, and α_m of peak Ni_2 is not influenced by the contraction of $\Delta d_{12}/d_B$. In Fig. 7, the larger the contraction of first interlayer spacing is, the smaller the peak position α_m of $Ni_{2''}$ is. For an inward relaxation of 40%, the superposition of peaks $Ni_{2'}$ and $Ni_{2''}$ produces the single peak Ni_2 with $\alpha_m = 38°$.

Fig. 8 shows the ACOCT results of 180° Li NICISS intensity from Al atoms against α for the various inward-relaxation values of first interlayer spacing. Owing to the inward relaxation, the peak intensity Al_1 and the peak position α_m of Al_1 decrease, and the peak width (FWHM) $\Delta\alpha$ of peak Al_1 becomes broader. As is supposed in Figs. 6a and 6b, whereas α_m of the peak Al_1, which originates from the focusing effect by third-layer Ni atoms onto fourth-layer Al atoms, is scarcely dependent on the inward relaxation of first interlayer spacing, the peak positions α_m of peaks Al_1, which are due to the focusing effects from first-layer Ni atoms onto second-layer Al atoms and from first-layer Ni atoms onto sixth-layer Al atoms, decrease by the contraction of first interlayer spacing. Consequently, in Fig. 8, the peak intensity Al_1 and α_m of peak Al_1 for contraction of $\Delta d_{12}/d_B = 20 - 40\%$ become smaller than those for no relaxation and $\Delta\alpha$ of peak Al_1 for contraction of $\Delta d_{12}/d_B = 20 - 40\%$ becomes broader than that for no relaxation. Fig. 9 shows the peak positions α_m as a function of $\Delta d_{12}/d_B$. In the 180° Li NICISS intensity, the peak positions α_m of peaks from not only Ni atoms but also Al atoms are strongly dependent on $\Delta d_{12}/d_B$. Therefore, in the following we discuss the influence of multilayer relaxation with Ni atoms at the outermost layer of NiAl(111) surface on the 180° Li NICISS intensity.

The multilayer relaxation of first and second interlayer spacings on Ni terminated layer at the NiAl(111) surface is taken into account in the present ACOCT code. We adopted $\Delta d_{12}/d_B = -40\%$ determined previously by the ACOCT results of 180° He NICISS intensity[16] as the relaxation value of first interlayer spacing. Fig. 10 shows the ACOCT results of 180° Li NICISS intensity from Ni atoms versus α for the various relaxation values $\Delta d_{23}/d_B$. The peak position α_m of Ni_2 becomes smaller as the contraction of second interlayer spacing becomes larger, and α_m of peak Ni_2 increases with increasing the outward-relaxation value of $\Delta d_{23}/d_B$. The reason why α_m of 180° Li NICISS intensity from Ni atoms in Fig. 10 is dependent on $\Delta d_{23}/d_B$ is due to the 180° backscattering from seventh-layer Ni atoms, because the trajectory Ni_2, which is schematically delineated in Fig. 11, is affected by the relaxation of second interlayer spacing, i.e. of second-layer Al atoms. Namely, the larger the outward relaxation of second interlayer spacing is, the larger the peak position α_m for the trajectory Ni_2 attributable to the focusing from second-layer Al atoms onto seventh-layer Ni atoms

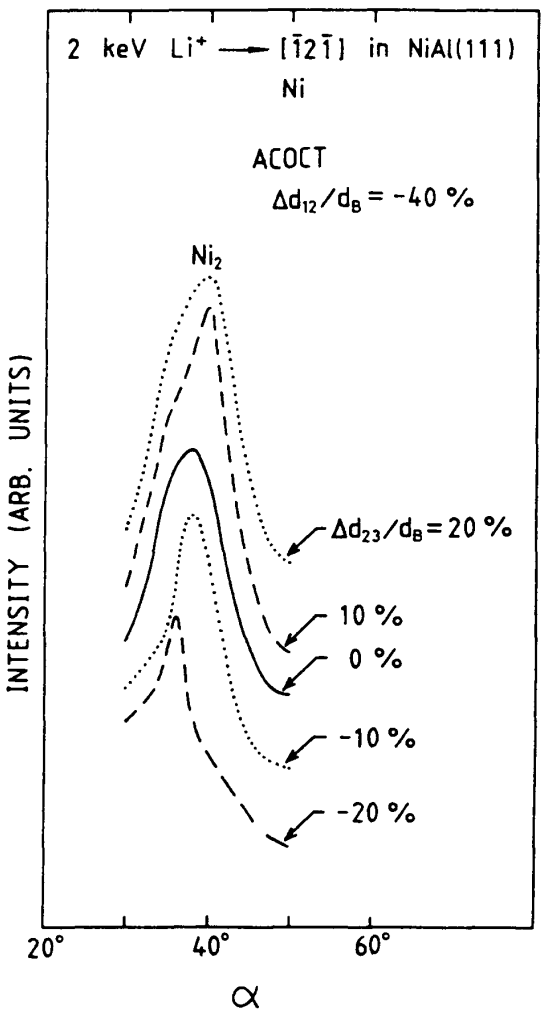

Fig. 10 ACOCT results of dependence of 180° Li NICISS intensity from Ni atoms at a NiAl(111) surface on α for various relaxation values $\Delta d_{23}/d_B$, where the notation Ni_2 of peak is equivalent to that in Fig. 7.

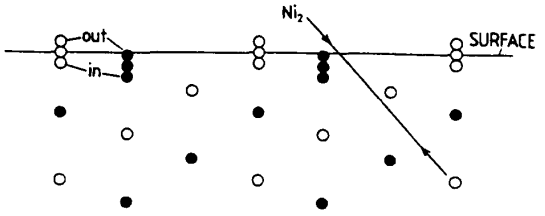

Fig. 11 Schematic trajectory Ni_2 of 180° Li particles backscattered from seventh-layer Ni atoms at a NiAl(111) surface for the relaxation of second interlayer spacing, where the inward relaxation of $\Delta d_{12}/d_B$ is taken into account in this figure, the notation Ni_2 of trajectory corresponds to that of peak in Fig. 10, the notations "in" and "out" denote the inward and outward relaxations, respectively.

is, and α_m for same trajectory Ni_2 decreases with increasing the inward-relaxation value of $\Delta d_{23}/d_B$. In this case, the 180° Li NICISS intensity from fifth-layer Ni atoms is larger than that from seventh-layer Ni atoms. However, the peak position α_m of single peak Ni_2 due to the superposition of peaks $Ni_{2'}$ and $Ni_{2''}$ from fifth-layer Ni atoms for $\Delta d_{12}/d_B=-40\%$ is scarcely dependent on the relaxation value $\Delta d_{23}/d_B$, because α_m of peak $Ni_{2'}$, which is independent of the relaxation of first-layer Ni atoms, is the lower limit of α_m of peak Ni_2 (see Fig. 3b).

Fig. 12 represents the ACOCT results of 180° Li NICISS intensity from Al atoms versus α for the various relaxation vaues $\Delta d_{23}/d_B$. The larger the outward-relaxation value of $\Delta d_{23}/d_B$ is, the larger the peak position α_m of Al_1 becomes, and α_m of peak Al_1 becomes smaller as the inward-relaxation value of $\Delta d_{23}/d_B$ increases. The shifting of α_m of 180° Li NICISS intensity from Al atoms in Fig. 12 is attributed to the 180° backscattering from sixth-layer Al atoms. This is explained as follows using Fig. 13. Even if only the relaxation value $\Delta d_{23}/d_B$ varies for the constant value of $\Delta d_{12}/d_B=-40\%$, the positions of first-layer Ni atoms are displaced from the surface of $\Delta d_{23}/d_B=0\%$ to the inner or outer side of a crystalline target. Thus, the peak position α_m of peak Al_1 due to the focusing effect from first-layer Ni atoms onto sixth-layer Al atoms increases as the outward-relaxation value of $\Delta d_{23}/d_B$ becomes larger, and α_m of peak Al_1 decreases with increasing the inward-relaxation value of $\Delta d_{23}/d_B$. Although the 180° Li NICISS intensity from fourth-layer Al atoms is larger than that from sixth-layer Al atoms, α_m of peak Al_1 from fourth-layer Al atoms is hardly dependent on $\Delta d_{12}/d_B$ and $\Delta d_{23}/d_B$, because the intensity peak Al_1 from fourth-layer Al atoms is due to the focusing effect by third-layer Ni atoms onto fourth-layer Al atoms (see Fig. 6a).

Fig. 14 shows α_m of the simulated 180° Li NICISS intensity from Ni and Al atoms versus $\Delta d_{23}/d_B$ using the ACOCT code, where $\Delta d_{12}/d_B=-40\%$. The peak positions α_m of peaks due to not only Ni atoms but also Al atoms are strongly dependent on $\Delta d_{23}/d_B$. Moreover, let us discuss that the simulated 180° Li NICISS intensity using the ACOCT code gives the very interesting results. The addition of the relaxation values of first and second interlaye spacings is equivalent to the relaxation value $\Delta d_{13}/d_B$ (in %) of spacing, d_{13}, between first- and third-layer atoms, i.e.,

$$\Delta d_{13}/d_B=\Delta d_{12}/d_B+\Delta d_{23}/d_B, \tag{1}$$

where $\Delta d_{13}/d_B$ is also represented as $\Delta d_{13}/d_B=(d_{13}-2d_B)/d_B$. By substituting the peak positions α_m versus $\Delta d_{12}/d_B$ and versus $\Delta d_{23}/d_B$ shown in Figs. 9 and 14 into Eq.(1), we can distinguish $\alpha_m=40°$ for $\Delta d_{13}/d_B=-20\%$ with $\Delta d_{12}/d_B=-40\%$ and $\Delta d_{23}/d_B=+20\%$ from $\alpha_m=35°$ and 40° for $\Delta d_{13}/d_B=-20\%$ with $\Delta d_{12}/d_B=-20\%$ and $\Delta d_{23}/d_B=0\%$, and $\alpha_m=40°$ for $\Delta d_{13}/d_B=-30\%$ with $\Delta d_{12}/d_B=-40\%$ and $\Delta d_{23}/d_B=+10\%$ from $\alpha_m=35°$ and 39° for $\Delta d_{13}/d_B=-30\%$ with $\Delta d_{12}/d_B=-30\%$ and $\Delta d_{23}/d_B=0\%$ in the 180° Li NICISS intensity from Ni atoms, and we can also discriminate $\alpha_m=44°$ for $\Delta d_{13}/d_B=-20\%$ with $\Delta d_{12}/d_B=-40\%$ and $\Delta d_{23}/d_B=+20\%$ from $\alpha_m=43°$ for $\Delta d_{13}/d_B=-20\%$ with $\Delta d_{12}/d_B=-20\%$ and $\Delta d_{23}/d_B=0\%$, and $\alpha_m=43°$ for $\Delta d_{13}/d_B=-30\%$ with $\Delta d_{12}/d_B=-40\%$ and $\Delta d_{23}/d_B=+10\%$ from $\alpha_m=42°$ for $\Delta d_{13}/d_B=-30\%$ with $\Delta d_{12}/d_B=-30\%$ and

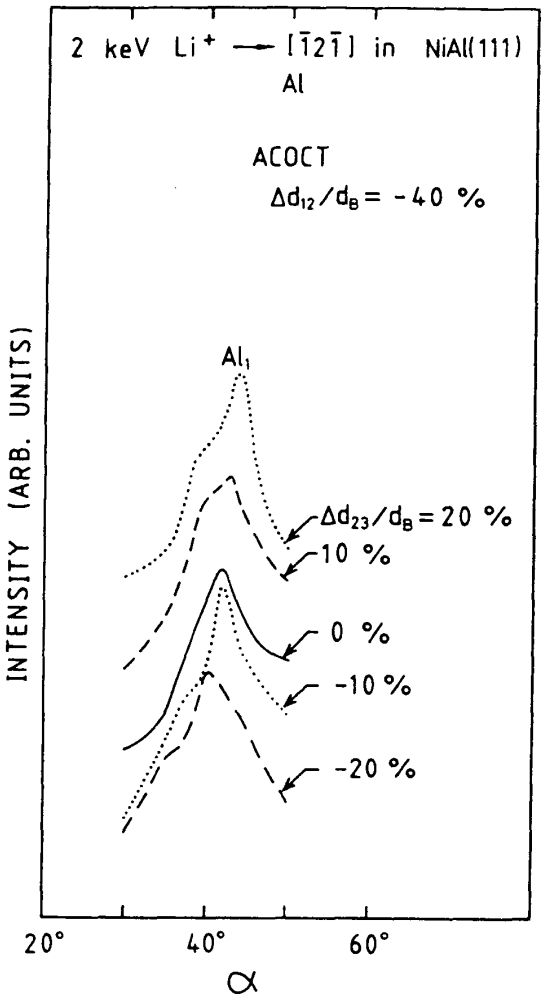

Fig. 12 Simulated 180° Li NICISS intensity from Al atoms at a NiAl(111) surface versus α for various relaxation values $\Delta d_{23}/d_B$ using the ACOCT code, where the notation Al_1 of peak corresponds to that in Fig. 8.

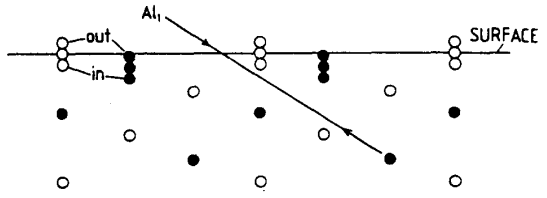

Fig. 13 Schematic trajectory Al_1 of 180° Li particles backscattered from sixth-layer Al atoms at a NiAl(111) surface for the relaxation of second interlayer spacing, where the inward relaxation of $\Delta d_{12}/d_B$ is taken into account in this figure, the notation Al_1 of trajectory is equivalent to that of peak in Fig. 12.

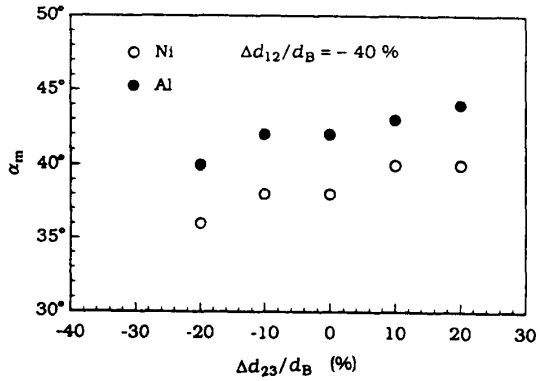

Fig. 14 ACOCT results of peak positions α_m of 180° Li NICISS intensity from Ni and Al atoms at a NiAl(111) surface versus $\Delta d_{23}/d_B$.

$\Delta d_{23}/d_B = 0\%$ in the 180° Li NICISS intensity from Al atoms. Accordingly, these ACOCT results imply that there is the possibility of estimaion of the multilayer relaxation on Ni terminated domain at the NiAl(111) surface with the 180° Li NICISS data.

4. Conclusion

Noonan and Davis have evaluated the multilayer relaxation at the NiAl(111) surface in LEED analysis. It is desirable to analyze the multilayer relaxation at this surface by employing other methods of measurements besides LEED for the sake of more perfect demonstration of the surface structural analysis. Thus, we examined the possibility of entimation of the multilayer relaxation on Ni terminated domain at the NiAl(111) surface with the 180° NICISS data using the ACOCT computer code based on BCA,

where the projectiles employed in the present ACOCT code are Li^+ ions of 2 keV. From the ACOCT results of 180° Li NICISS intensity versus angle of incidence between the ion beam and the target surface, it was found that peak positions of peaks from not only Ni atoms but also Al atoms are strongly dependent on the relaxation values of first and second interlayer spacings. As a result, it is possible to estimate the multilayer relaxation on Ni terminated layer at the NiAl(111) surface with the 180° Li NICISS data. Therefore, we desire that the data of 180° Li NICISS intensity versus angle of incidence are given by the 180° NICISS measurements.

References

1) H. Niehus, W. Heiland and E. Taglauer, Surf. Sci. Rep. **17** (1993) 213.
2) M. Aono, C. Oshima, S. Zaima, S. Otani and Y. Ishizawa, Jpn. J. Appl. Phys. **20** (1981) L829.
3) M. Aono, Nucl. Instr. and Meth. **B2** (1984) 374.
4) M. Katayama, E. Nomura, N. Kanekawa, H. Soejima and M. Aono, Nucl. Instr. and Meth. **B33** (1988) 857.
5) M. Aono, M. Katayama, E. Nomura, T. Chassé, D. Choi and M. Kato, Nucl. Instr. and Meth. **B37/38** (1989) 264.
6) H. Niehus and G. Comsa, Surf. Sci. **152/153** (1985) 93.
7) H. Niehus and G. Comsa, Nucl. Instr. and Meth. **B15** (1986) 122.
8) H. Niehus, J. Vac. Sci. Technol. **A5** (1987) 751.
9) H. Niehus, Surf. Sci. **166** (1986) L107.
10) H. Niehus, Nucl. Instr. and Meth. **B33** (1988) 876.
11) R. Spitzl, H. Niehus and G. Comsa, Rev. Sci. Instr. **61** (1990) 760.
12) H. Niehus, W. Raunau, K. Besocke, R. Spitzl and G, Comsa, Surf. Sci. Lett. **225** (1990) L8.
13) J.R. Noonan and H.L. Davis, Phys. Rev. Lett. **59** (1987) 1714.
14) J.R. Noonan and H.L. Davis, J. Vac. Sci. Technol. **A6** (1988) 722.
15) S.H. Overbury, D.R. Mullins and J. F. Wendelken, Surf. Sci. **236** (1990) 122.
16) W. Takeuchi and Y. Yamamura, Nucl. Instr. and Meth. **B84** (1994) 443.
17) Y. Yamamura and W. Takeuchi, Nucl. Instr. and Meth. **B29** (1987) 461.
18) Y. Yamamura and W. Takeuchi, Research Report IPPJ-848, Institute of Plasma Physics, Nagoya University, Japan (1987).
19) R.J. Kobistek, G. Bozzolo, J. Ferrante and H. Schlosser, Surf. Sci. **307-309** (1994) 390, and references therein.
20) G. Molière, Z. Naturforsch. **2a** (1947) 133.
21) O.B. Firsov, Sov. Phys. JETP **6** (1958) 534.
22) D.S. Gemmell, Rev. Mod. Phys. **46** (1974) 129.
23) W. Takeuchi and Y. Yamamura, Nucl. Instr. and Meth. **B2** (1984) 336.
24) W. Takeuchi and Y. Yamamura, Surf. Sci. **169** (1986) 365.
25) W. Takeuchi and Y. Yamamura, Surf. Sci. **277** (1992) 351.
26) W. Takeuchi and Y. Yamamura, Nucl. Instr. and Meth. **B72** (1992) 363.
27) Y. Wang, M. Shi and J.W. Rabalais, Nucl. Instr. and Meth. **B62** (1992) 505.
28) D.R. Mullins and S.H. Overbury, Surf. Sci. **199** (1988) 141.
29) S.H. Overbury and D.R. Huntley, Phys. Rev. **B32** (1985) 6278.
30) S.H. Overbury, Surf. Sci. **175** (1986) 123.